Formation of Nitric Acid in the Gas-Phase HO_2 + NO Reaction: Effects of Temperature and Water Vapor

N. I. Butkovskaya,*,† A. Kukui,‡ N. Pouvesle,† and G. Le Bras†

CNRS, Laboratoire de Combustion et Systèmes Réactifs, 1C Av. de la Recherche Scientifique, 45071 Orléans Cedex 2, France, and CNRS, Service d'Aéronomie, Paris, France

Received: March 24, 2005; In Final Form: May 30, 2005

A high-pressure turbulent flow reactor coupled with a chemical ionization mass spectrometer was used to investigate the minor channel (1b) producing nitric acid, HNO_3, in the HO_2 + NO reaction for which only one channel (1a) is known so far: HO_2 + NO → OH + NO_2 (1a), HO_2 + NO → HNO_3 (1b). The reaction has been investigated in the temperature range 223−298 K at a pressure of 200 Torr of N_2 carrier gas. The influence of water vapor has been studied at 298 K. The branching ratio, k_{1b}/k_{1a}, was found to increase from $(0.18^{+0.04}_{-0.06})$% at 298 K to $(0.87^{+0.05}_{-0.08})$% at 223 K, corresponding to $k_{1b} = (1.6 \pm 0.5) \times 10^{-14}$ and $(10.4 \pm 1.7) \times 10^{-14}$ cm^3 molecule^{-1} s^{-1}, respectively at 298 and 223 K. The data could be fitted by the Arrhenius expression $k_{1b} = 6.4 \times 10^{-17} \exp((1644 \pm 76)/T)$ cm^3 molecule^{-1} s^{-1} at $T = 223-298$ K. The yield of HNO_3 was found to increase in the presence of water vapor (by 90% at about 3 Torr of H_2O). Implications of the obtained results for atmospheric radicals chemistry and chemical amplifiers used to measure peroxy radicals are discussed. The results show in particular that reaction 1b can be a significant loss process for the HO_x (OH, HO_2) radicals in the upper troposphere.

1. Introduction

The HO_2 + NO reaction occurs in radical chemical amplifiers [e.g., 1−4] to convert low concentrations of HO_2 into measurable NO_2 concentrations in a chain reaction (1−3):

$$HO_2 + NO \rightarrow OH + NO_2 \quad (1a)$$

$$OH + CO \rightarrow H + CO_2 \quad (2)$$

$$H + O_2 + M \rightarrow HO_2 + M \quad (3)$$

Chain termination takes place mainly through the gas-phase reaction

$$HO + NO + M \rightarrow HONO + M \quad (4)$$

and the HO_2 radical wall loss. It was found that the chain length decreases in the presence of water vapor and that the expected increase of HO_2 wall losses may account for only some part of the observed water effect.[1,2] It has been suggested that this effect could be, at least partially, attributed to the reaction of the $HO_2 \cdot H_2O$ adduct with NO yielding nitric acid, HNO_3, or peroxynitrous acid, HOONO.[2] Recently, a detailed study of the phenomena resulting in a chain termination provided additional evidence that formation of nonradical products (e.g., HNO_3) in the HO_2 + NO reaction in the presence of water is likely to be responsible for the chain shortening.[4]

The initial aim of the present work was to clarify this problem by studying the possible formation of HNO_3, or its isomer HOONO, as a minor channel of the HO_2 + NO reaction in the presence of water:

$$HO_2 + NO + H_2O \rightarrow HNO_3 \text{ (or HOONO)} + H_2O$$

The observation of HNO_3 in reaction 1 at room temperature, at very low but measurable yield, even in the absence of H_2O, led us to extend the study to low temperatures. An increase of the HNO_3 yield with decreasing temperature being possible, reaction 1b

$$HO_2 + NO + M \rightarrow HNO_3 + M \quad (1b)$$

may become a significant sink of HO_x (OH, HO_2) in the upper troposphere.

Reaction of HO_2 with NO is very important in atmospheric chemistry because of its central role in the OH/HO_2 recycling and reduction of ozone depletion by HO_x cycles in the stratosphere and in ozone production in the troposphere. The importance of this reaction was demonstrated by Howard and Evenson[5] who carried out the first direct measurement of its rate constant. Further studies covering atmospheric conditions[6−9] established a negative temperature dependence of the rate constant in the 183−403 K range with a recommended value of $(8.8 \pm 1.2) \times 10^{-12}$ cm^3 molecule^{-1} s^{-1} at 298 K.[10] The reaction is supposed to proceed via the formation of the excited HOONO intermediate complex followed by rapid decomposition to OH and NO_2:

$$HO_2 + NO \rightarrow HOONO^{**} \rightarrow OH + NO_2 \quad (1a)$$

Howard[6] considered two competing channels, stabilization of HOONO complex and formation of HNO + O_2:

* Permanent address: Institute of Chemical Physics of the Russian Academy of Sciences, 117334 Moscow, Russian Federation.
† CNRS, Laboratoire de Combustion et Systèmes Réactifs.
‡ CNRS, Service d'Aéronomie.

10.1021/jp051534v CCC: $30.25
Published on Web 07/01/2005

$$HO_2 + NO + M \rightarrow HOONO + M$$

$$HO_2 + NO \rightarrow HNO + O_2$$

The upper limit for each of these channels was estimated to be lower than 0.13% from the measurement of OH and HO_2 concentrations as a function of reaction time at $P = 1-3$ Torr and $T = 271$ and 303 K using a laser magnetic resonance method. The predominance of channel 1a was confirmed by Bohn and Zetzsch,[8] who obtained for the $HO_2 + NO$ reaction a quantum yield of OH $\geq$ 95% using time-resolved detection of OH by CW UV-laser absorption at $P = 75$, 375, and 750 Torr. They argued that stabilization of HOONO with possible further rearrangement to HNO_3

$$HO_2 + NO + M \rightarrow HOONO^{**} + M \rightarrow HOONO + M \rightarrow HNO_3 + M$$

seemed to be unlikely at atmospheric pressures but could not be excluded totally. In the recent work of Bardwell et al.[9] a (100 $\pm$ 5)% yield of NO_2 was obtained using the chemical ionization mass spectrometry (CIMS) technique. No stabilized adducts or secondary product channels were observed within the error limits of their study over the 183−300 K temperature range. Because of its atmospheric importance, the formation of organic nitrates in $RO_2 + NO$ reactions is a topic of intense interest (see Discussion). It is interesting to mention that if the $HO_2 + NO$ reaction produces HNO_3, it becomes a part of the family of peroxy radical reactions with NO that produce nitrates.

In the present work, the branching fraction and the kinetics of nitric acid formation in the $HO_2 + NO$ reaction were investigated by direct detection of HNO_3 by CIMS at 298 K in the absence and presence of H_2O and in the temperature range 298−223 K without H_2O. All the experiments were carried out at $P = 200$ Torr of N_2, except a few ones in the range of 100−400 Torr as a test of the HNO_3 formation mechanism.

2. Experimental Method

2.1. Main Reactor. The title reaction was studied in a high-pressure turbulent flow reactor (HPTFR) coupled with an ion−molecule reactor and a quadrupole mass spectrometer (Figure 1). The pressure in the reactor (Pyrex tube of 2.4 cm i.d.) was 200 Torr; flow velocity of N_2 carrier gas was about 17 m/s. The total flow through the reactor was up to 96 SLPM. Mixing and flow conditions were determined by a Reynolds number of Re $\approx$ 7300, which ensured fast turbulent mixing of reagents and a flat radial velocity profile. A detailed description of the experimental setup is presented elsewhere.[11] NO was introduced into the reactor upstream of the tip of the movable injector of 1.1 cm i.d. which served as a prereactor for producing HO_2 radicals from the $H + O_2$ reaction. H-atoms were generated by microwave discharge in a H_2/He gas mixture in a quartz tube of 0.6 cm i.d. concentrically connected with the injector. He (Alpha Gaz 2) was purified by passing through the molecular sieves cooled by liquid N_2. Concentration of molecular oxygen (Alpha Gaz 2) in the injector (1.5×10^{16} molecule cm^{-3}) was sufficient to consume the H-atoms entirely during the $\sim$2 ms residence time in the injector. Typical HO_2 concentrations in the main reactor were $(2-5) \times 10^{11}$ molecule cm^{-3}. The maximal distance from the injector tip to the orifice of the inlet cone of the ion−molecule reactor was $L = 50$ cm corresponding to a reaction time of $t \approx 30$ ms. The cooling of the reactor was achieved by immersing a metal coil with the carrier gas into a Dewar vessel filled with liquid nitrogen. The temperature was regulated using an RKC Instrument CB100 digital controller.

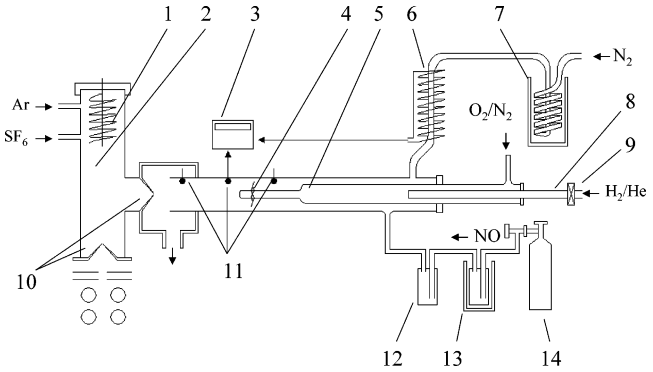

Figure 1. Experimental setup: (1) ion source; (2) ion molecule reactor (IMR); (3) temperature controller; (4) "turbulizer"; (5) injector; (6) resistance; (7) liquid N_2 cooling bath; (8) discharge tube; (9) microwave discharge; (10) sampling cones; (11) temperature sensors; (12) $Fe^{II}(SO_4)$ sieves; (13) liquid N_2/ethanol cooling bath; (14) NO cylinder.

A T-type thermocouple inserted in the middle of the reactor served as a temperature input of the controller. Two K-type thermocouples were used to measure the temperature at both ends of the reactor.

The NO flow rate was varied from 0.05 to 120 SCCM using two TYLAN flow controllers; the corresponding concentrations in the reactor were from 5.0×10^{12} to 1.2×10^{16} molecule cm^{-3}. The tank grade NO (AlphaGaz N20) passed successively through three ethanol/liquid N_2 cooled traps and an iron sulfate filter to remove NO_2 and heavier nitrogen oxides. At $P = 200$ Torr, detection of HNO_3 from reaction 1 was complicated by the secondary reaction 5:

$$OH + NO_2 + M \rightarrow HNO_3 + M \qquad (5)$$

To suppress this reaction, OH radicals were scavenged by high concentrations of NO or cyclohexane.

Cyclohexane entered the reactor with the He flow passing through the trap with liquid C_6H_{12} (Riedel de Haën, > 99.5%), which was preliminarily purified in several freeze−pump−thaw cycles. Water vapor in experiments at 298 K was introduced into the reactor together with a part of N_2 flow bubbling through distilled H_2O in the stainless steel reservoir of 25 cm height. The reservoir was placed in the cryostat maintained at a constant temperature of 19 °C. Assuming that the partial water pressure in the flow was equal to the saturated vapor pressure, the estimated water concentration in the reactor varied from 1×10^{16} to 1.17×10^{17} molecule cm^{-3}.

2.2. Chemical Ionization. The ion−molecule reactor (IMR) consisted of a stainless steel tube of 4 cm i.d. and 40 cm length situated perpendicular to the chemical reactor. Ar (Alpha Gaz 2) was used as a carrier gas in the IMR at a flow rate of 2.2 SLPM and pressure of about 1 Torr. This gave an average flow velocity of 44 m/s and a reaction time of the order of 4 ms. The carrier gas was purified by passing through liquid N_2 cooled traps. Electrons were generated by electrical heating of a thoriated irridium filament. Primary Ar^+ ions were produced by electron bombardment. SF_6 (Alpha Gaz N37) was introduced into the IMR downstream of the filament. The SF_6^- negative ions were produced by attachment of thermalized electrons to SF_6.

Two chemical ionization methods were used to detect HNO_3: at *m*/*e* 82 using the fast ion−molecule reaction 1i as suggested by Huey et al.,[12]

$$SF_6^- + HNO_3 \rightarrow [NO_3^- \cdot HF] + SF_5 \qquad (1i)$$

and at *m*/*e* 186 using reaction 2i originally described by Huey and Lovejoy,[13a]

$$SiF_5^- + HNO_3 \rightarrow [SiF_5^- \cdot HNO_3] \quad (2i)$$

the latter being used for HNO_3 atmospheric measurements.[13b] SiF_5^- ions were produced by fast transfer reaction 3i when SiF_4 (Air Products 99,94%) was added to SF_6 flow:

$$SF_6^- + SiF_4 \rightarrow SiF_5^- + SF_5 \quad (3i)$$

However, at low pressure in the ion molecule reactor, the sensitivity to HNO_3 using SiF_4 is substantially lower than that using SF_6,[12,13a] and this detection method was employed in our study only in order to prove that the signal observed as a product of 1b corresponds to HNO_3.

OH (*m*/*e* 17), NO_2 (*m*/*e* 46), and O_3 (used to test the system, *m*/*e* 48) were ionized by the charge-transfer reactions with SF_6^-:[12,14]

$$SF_6^- + OH \rightarrow OH^- + SF_6 \quad (4i)$$

$$SF_6^- + NO_2 \rightarrow NO_2^- + SF_6 \quad (5i)$$

$$SF_6^- + O_3 \rightarrow O_3^- + SF_6 \quad (6i)$$

HO_2 radicals could be detected at *m*/*e* 140 using reaction[15]

$$SF_6^- + HO_2 \rightarrow [SF_4 \cdot O_2]^- + \text{other products} \quad (7i)$$

In this work we also show that HONO can be detected at *m*/*e* 66 and *m*/*e* 170 using reactions (see also ref 11, Figure 8)

$$SF_6^- + HONO \rightarrow [HF \cdot NO_2^-] + SF_5 \quad (8i)$$

$$SiF_5^- + HONO \rightarrow [SiF_5^- \cdot HONO] \quad (9i)$$

The relative sensitivities were approximately $S(NO_2)$:S(OH):$S(HNO_3)$:S(HONO) = 1.0:5.5:4.5:3.0 with SF_6^-. The 2σ detection limits for integration time of 20 s were 3.2×10^9 (NO_2), 2.5×10^8 (OH), 2.5×10^8 (HNO_3), and 2.3×10^8 (HONO) molecule cm^{-3} using SF_6^- and 5.6×10^8 (HNO_3) molecule cm^{-3} using SiF_5^-.

2.3. Calibration of Signals. 2.3.1. NO_2. The NO_2 signal from reaction 1 was calibrated by introducing known concentrations of NO_2 into the reactor. The NO_2 flow rate was determined from measurement of the pressure drop in a known volume when a preprepared NO_2/He mixture was passing into the reactor via a regulating valve. The mixtures were prepared by mixing either NO or gaseous NO_2 (MATHESON) (60−100 Torr) with O_2 (1 atm) in a glass flask which was kept for 1 day and night to allow NO to react with oxygen. Then, NO_2 was purified by condensation at liquid N_2 temperature and pumping away the excess O_2 at a pressure of about 50 Torr. He, purified by passing through the liquid N_2 cooled trap with molecular sieves, was added into the flask to get a total pressure slightly over 1 atm to obtain a 1% NO_2/He mixture in one flask and 7−12% mixture in another one. The 1% mixture was used to calibrate OH radicals. The presence of N_2O_4 dimer in the NO_2 mixture was taken into account in the calculation of NO_2 concentration in the reactor. The signal intensity at *m*/*e* 46 showed linear dependence on the measured NO_2 flow in the $[NO_2] = (0.02-3) \times 10^{13}$ molecule cm^{-3} range in the main reactor. When the NO_2/He mixture was introduced through the movable injector, the mass spectral response did not depend on the position of the injector when L was changed from 3 to 50 cm, confirming the constant NO_2 concentration over the reactor cross section.[11]

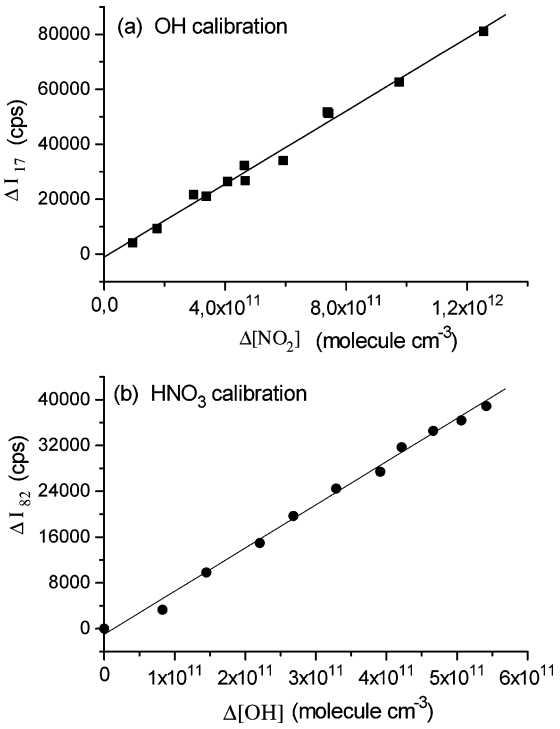

Figure 2. Calibration of OH radicals from H + NO_2 reaction measuring NO_2 consumption (a) and calibration of HNO_3 from the OH + NO_2 reaction measuring OH consumption (b).

2.3.2. HO_2. HO_2 signal was quantified during the HO_2 + NO reaction at sufficiently high NO concentration, when all HO_2 radicals were converted to NO_2. The reaction channel with HNO_3 formation may be neglected for the purpose of HO_2 calibration.

2.3.3. OH. Determination of the concentrations of other species involved in the study was based on NO_2 calibration using the fast reaction 7 followed by reactions 4 and 5

$$H + NO_2 \rightarrow OH + NO \quad (7)$$

$$HO + NO + M \rightarrow HONO + M \quad (4)$$

$$OH + NO_2 + M \rightarrow HNO_3 + M \quad (5)$$

with the rate constants $k_4 = (3.0 \pm 0.5) \times 10^{-12}$ [16] and $k_5 = (6.4 \pm 0.4) \times 10^{-12}$ cm^3 $molecule^{-1}$ s^{-1} at 298 K and 200 Torr.[17] NO_2 was introduced into the main reactor upstream of the H-atoms injector. At low NO_2 concentrations and short reaction times, reactions 4 and 5 can be ignored and calibration of OH radicals can be done by measuring NO_2 consumption at different NO_2 flow rates. In this case $\Delta[OH] = \Delta[NO_2]$. At $t \approx 5$ ms the linearity between the OH signal intensity and NO_2 consumption holds up to $[NO_2] \approx 2 \times 10^{12}$ molecule cm^{-3} (Figure 2a).

2.3.4. HNO_3. A direct calibration by preparing a standard synthesized sample of HNO_3 was not successful because of the difficulties to introduce HNO_3 into the reactor.[18] Linearity of the mass spectrometric signal from the 5% mixture of HNO_3 vapor in He introduced into the reactor was not reached even for the largest available flow rate corresponding to $[HNO_3] = 5 \times 10^{13}$ molecule cm^{-3}. That is why calibration of HNO_3 was made by producing HNO_3 in situ via reactions 7 and 5. Time profiles of NO_2 and reaction product concentrations are presented in Figure 3. In this example the initial concentration of

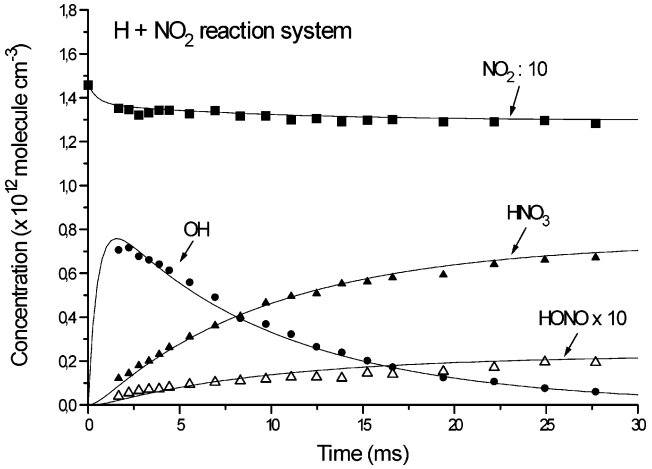

Figure 3. Concentration−time profiles of the species in the H + NO_2 reaction. Solid curves are the calculated profiles with initial concentrations $[NO_2]_0 = 1.5 \times 10^{13}$ and $[H]_0 = 9.0 \times 10^{11}$ molecule cm^{-3}.

NO_2 (1.5×10^{13} molecule cm^{-3}) was sufficient to consume most of the OH radicals. Figure 2b shows the dependence of the HNO_3 signal intensity on the change of OH concentration at reaction times between 4 and 22 ms obtained from the data presented in Figure 3. First, the OH signal was calibrated as described above. The dependence is linear and allows us to determine the sensitivity of the mass-spectrometric detection for HNO_3. In principle, to determine the branching ratio of reaction 1 we do not need absolute sensitivities for NO_2 and HNO_3 but only its ratio, which is directly provided by reaction 5. Yet, it is difficult to measure accurately small differences in NO_2 concentration (Figure 3), and calibration by OH signal is preferable.

The errors inherent to the HNO_3 calibration using reactions 7−5 have been considered in detail. Figure 3 illustrates the inaccuracies resulting from the incompleteness of reaction 5 and unaccounted OH losses. At sufficiently high NO_2 concentration and long reaction time, the OH radicals produced in reaction 7 are totally converted into HNO_3, and the HNO_3 concentration could be calculated as $[HNO_3] = \Delta[NO_2]/2$. In such a case HNO_3 can be calibrated without doing OH calibration. The measured NO_2 consumption at $t = 28$ ms was $\Delta[NO_2] = 1.57 \times 10^{12}$ molecule cm^{-3}. Rough estimation of formed HNO_3 gives $[HNO_3] = \Delta[NO_2]/2 = 7.9 \times 10^{11}$ molecule cm^{-3}. Account for the nonreacted OH (9%) gives $[HNO_3] = \Delta[NO_2]\cdot(1-0.09)/(2-0.09) = (7.5 \pm 1.3) \times 10^{11}$ molecule cm^{-3}, where the error limits are defined by the noise of the NO_2 signal. Using calibration from Figure 2b, we obtain for the HNO_3 final concentration a very close value of $(7.3 \pm 0.4) \times 10^{11}$ molecule cm^{-3}, where the error limits are the 2σ of the slope of the calibration curve in Figure 2b. Simulation of the kinetic profiles of the products shows that the errors in HNO_3 calibration using OH signal is due mainly to the OH wall loss (∼5%), whereas the OH + OH and OH + NO reactions account for another 4% and 2%, respectively. The calculated time profiles with $[H]_0 = 9 \times 10^{11}$ molecule cm^{-3} are shown in Figure 3. The reaction scheme used to simulate the H + NO_2 chemical system is presented in Table 1. The wall loss $k_w = 14 \pm 1$ s^{-1} was measured in independent experiments. As a rule, calibration of HNO_3 was made using higher NO_2 concentrations ($[NO_2] = (1.6-2.5) \times 10^{13}$ molecule cm^{-3}), to get a faster completion of reaction 5 and thus to decrease wall loss and, with lower H-atom concentration ($[H] < 5 \times 10^{11}$ molecule cm^{-3}), to minimize OH loss by self-reaction. The resulting HNO_3 calibration uncertainty was within 10% including the experimental errors in the measurement of signal intensities.

Additional possible uncertainty is connected with a branching in reaction 5. According to recent studies of reaction 5, at 200 Torr and 298 K, formation of the HOONO isomer must be considered since the branching ratio of channel 5b might be up to 22%:[19−21]

$$OH + NO_2 + M \rightarrow HOONO + M \qquad (5b)$$

Although these data are in disagreement with those from other studies [e.g., 22, 23] where HOONO was not observed by IR spectroscopy, or with a LIF study[24] confirmed by a priori calculation[25] where extremely high pressures were needed for detection of HOONO, this possibility cannot be ignored. It was suggested[21,24,26] that the isomer is a long-lived molecule, which, then, might be detected in our experiments. The rate constant of reaction 1i is close to the calculated ADO (average dipole orientation) collisional rate constant.[12] So, the sensitivity for HOONO with detection using SF_6^- is expected to be either similar or less than that for HNO_3. If HOONO is detected with similar sensitivity as HNO_3, the HNO_3 calibration would not be perturbed. If it does not give a signal at *m*/*e* 82, the HNO_3 concentration would be overestimated. Hence, the uncertainty in the knowledge of whether the ion−molecule reaction of HOONO with SF_6^- can produce the $NO_3^-\cdot HF$ ion increases the lower uncertainty limit in the HNO_3 calibration to approximately 30%.

2.3.5. Detection of HNO_3 Using SiF_4. The sensitivities for HNO_3 provided by both reactions 1i and 2i were determined using the H + NO_2 reaction system (see Figure 3). Concentrations of SF_6^- and SiF_5^- ions in the IMR were monitored at their isotopic peaks $^{34}SF_6^-$ (*m*/*e* 148; 4.4% of the major isotope $^{32}SF_6^-$) and $^{29}SiF_5^-$ (*m*/*e* 124; 5.1% of the major isotope $^{28}SiF_5^-$) because of the possible saturation of the signals of the main isotopes. First, absolute sensitivities were measured with SF_6 in the IMR as described above. They were (in units of molecule cm^{-3}/cps) 6.6×10^7 (NO_2), 1.2×10^7 (OH), and 1.4×10^7 (HNO_3). The measured signal intensities are presented in the first line of Table 2. NO_2 intensity corresponds to the absence of reaction (discharge off), whereas HNO_3 intensity corresponds to the discharge on−off difference at maximal reaction time. The second line in Table 2 shows the change of intensities when SF_4 was added to SF_6 flow to give approximately equal amounts of the primary SF_6^- and SiF_5^- ions; the third line gives the intensities measured in excess of SiF_5^- over SF_6^-. As the concentrations in the main reactor were not changed, we obtain a relative sensitivity for HNO_3 detection with SF_6^- with respect to SiF_5^- of 22.9 ± 1.0. This ratio somewhat exceeds the one expected from the corresponding ion molecule reaction rate constants, $k_{1i} = (2 \pm 0.7) \times 10^{-9}$ cm^3 $molecule^{-1}$ s^{-1} [12] and $k_{2i} = (3.0 \pm 1) \times 10^{-10}$ cm^3 $molecule^{-1}$ s^{-1},[13a] which can be explained by the mass discrimination inherent to the instrument. The obtained sensitivity ratio was compared with that obtained in the HO_2 + NO system (see section 3.1).

2.3.6. Effect of H_2O on the Signal Intensities of HNO_3 (*m*/*e* 82) and NO_2 (*m*/*e* 46). A change of signal intensity at several masses including *m*/*e* 46 and 82 was observed when water vapor was introduced into the reactor. This effect was examined for different conditions: (1) N_2 carrier gas (background signals); (2) adding NO_2 and producing NO_2 from O_3 + NO reaction; (3) producing HNO_3 from OH + NO_2 reaction. Figure 4 shows the influence of different water concentrations on the intensity of mass spectral peaks at *m*/*e* 46 and 82. The results can be summarized as follows:

TABLE 1: Reaction Scheme Used to Simulate the H+ NO_2 and HO_2 + NO Chemical Systems

reaction	number in text	*k* (298 K, 200 Torr) cm^3 $molecule^{-1}$ s^{-1}	ref
	I. H + NO_2 System		
$H + NO_2 \rightarrow OH + NO$	(7)	1.3×10^{-10}	16
$OH + NO_2 + M \rightarrow HNO_3 + M$	(5)	6.4×10^{-12}	17
$OH + NO + M \rightarrow HONO + M$	(4)	3.0×10^{-12}	16
$OH + OH + M \rightarrow H_2O_2 + M$		2.7×10^{-12}	16
$OH + OH \rightarrow O + H_2O$		1.9×10^{-12}	16
$OH \rightarrow$ wall		14 s^{-1}	this work
	II. HO_2 + NO (+C_6H_{12}) System		
$HO_2 + NO \rightarrow OH + NO_2$	(1a)	8.8×10^{-12}	10
$HO_2 + NO + M \rightarrow HNO_3 + M$	(1b)	1.6×10^{-14}	this work
$OH + NO_2 + M \rightarrow HNO_3 + M$	(5)	6.4×10^{-12}	17
$OH + NO + M \rightarrow HONO + M$	(4)	3.0×10^{-12}	16
$HO_2 + HO_2 \rightarrow H_2O_2 + O_2$		1.7×10^{-12}	16
$OH + HO_2 \rightarrow H_2O + O_2$		1.1×10^{-10}	16
$OH \rightarrow$ wall		14 s^{-1}	this work
$HO_2 \rightarrow$ wall		10 s^{-1}	this work
$OH + C_6H_{12} \rightarrow C_6H_{11} + H_2O$	(6)	7.0×10^{-12}	51
$C_6H_{11} + O_2 + M \rightarrow C_6H_{11}O_2 + M$	(8)	1.3×10^{-11}	29
$C_6H_{11}O_2 + NO \rightarrow C_6H_{11}O + NO_2$	(9)	5.6×10^{-12}	29
$C_6H_{11}O_2 + NO \rightarrow C_6H_{11}ONO_2$		1.1×10^{-12}	29
$C_6H_{11}O_2 + NO_2 \rightarrow C_6H_{11}O_2NO_2$		9.5×10^{-12}	29
$C_6H_{11}O \rightarrow HC(O)(CH_2)_4CH_2$	(10)	6.3×10^4 s^{-1}	30
reactions 11−17: see text			

TABLE 2: Detection of NO_2, HNO_3 and HONO Using Ion−Molecule Reactions with SF_6^- and SiF_4^-

conditions in IMR	intensity (counts per second) SF_6^- *m/e* 148	SiF_5^- *m/e* 124	NO_2^- *m/e* 46	$HF{\cdot}NO_3^-$ *m/e* 82	$HNO_3{\cdot}SiF_4^-$ *m/e* 186
	I. H + NO_2 Reaction System; $[NO_2] = 8.0 \times 10^{12}$ molecule cm^{-3}				
only SF_6	442 843	219	122 846 (6.6×10^7)	**30 179** ± 522 (1.4×10^7)	n.o.[a]
$[SiF_5^-] \approx [SF_6^-]$	230 812	225 594	65 188	14 677	617
$[SiF_5^-] \gg [SF_6^-]$	27 344	418 094	8949	1402	**1316** ± 47 (3.43×10^8)[b] ***22.9*** ± ***1.0***[c]
	II. H + NO_2 Reaction System; $[NO_2] = 1.4 \times 10^{13}$ molecule cm^{-3}				
only SF_6			722 651 (2.0×10^7)[b]	140 223 (3.9×10^6)[b]	n.o.
$[SiF_5^-] \approx [SF_6^-]$			423 893	81 542	3064
	III. HO_2 + NO Reaction System; $[NO] = 9.3 \times 10^{14}$ molecule cm^{-3}				
only SF_6			21 184	**321** ± 35	n.o.
$[SiF_5^-] \approx [SF_6^-]$			13 088	211	7.7 ± 2.5
$[SiF_5^-] \gg [SF_6^-]$			2096	28.2	**15.5** ± 3.3 ***20.7*** ± ***5.0***[c]
	IV. HO_2 + NO Reaction System; $[NO] = 9.3 \times 10^{15}$ molecule cm^{-3}				
only SF_6			19 975	**129** ± 10	n.o.
$[SiF_5^-] \gg [SF_6^-]$			1986	11.6	**7.0** ± 2.3 ***18.4*** ± ***6.1***[c]

[a] "n.o." refers to "not observable". [b] Values in parentheses below intensities are reciprocal sensitivities in molecule cm^{-3}/cps. [c] Ratio of sensitivities for detection of HNO_3 with SF_6^- and SiF_5^-.

(1) NO_2 and background signal intensities at *m/e* 46 decrease with increasing water concentration in the range $(0-8) \times 10^{16}$ molecule cm^{-3}. This decrease is explained by the general drop of sensitivity when large concentrations of water are introduced into the main reactor. Inspection of spectra showed that introduction of water results in a decrease of SF_6^- ion concentration (nearly 30% decrease with $[H_2O] = 1.1 \times 10^{17}$ molecule cm^{-3}). Although it is known that SF_6^- ions react with H_2O,[27] the existing mechanism cannot explain such a large decrease of SF_6^- concentration, and this phenomenon needs further investigation.

(2) The signal of HNO_3 decreases in the presence of H_2O similarly to that of NO_2.

(3) The background signal at *m/e* 82 increases in the presence of H_2O. There is no unambiguous explanation of this increase. In principle, formation of nitric acid from H_2O and background NO_2 is possible on the walls of the reactor, IMR, or inlet tubes.[28] However, it was shown that HNO_3 does not leave the surface and, hence, cannot be detected in the gas phase.[28] It is more likely that the $NO_3^-{\cdot}HF$ ion is formed from the background NO_3^- ion and HF molecules (or complexes) produced in the IMR in the presence of H_2O.

3. Results

3.1. Detection of HNO_3 Using OH Scavenging by NO. Figure 5 shows the changes of NO_2 and HNO_3 concentrations with the increase of the concentration of NO from 1×10^{13} to 9.4×10^{15} molecule cm^{-3}. The measurements were done at $L = 45$ cm ($t = 29$ ms). As expected, NO_2 concentration increases

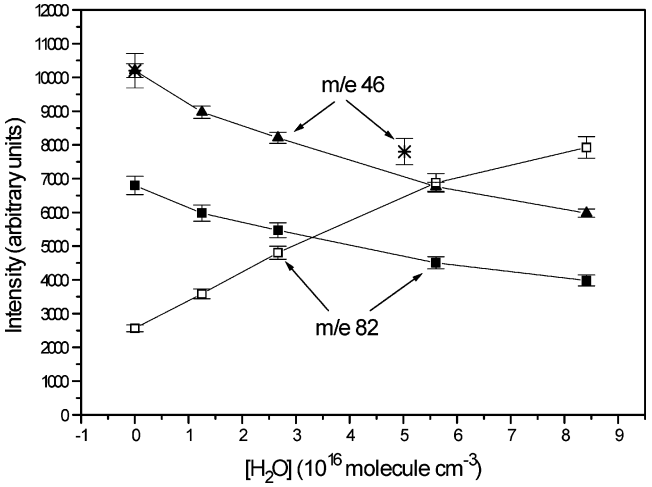

Figure 4. Water effect on mass spectrometric signal intensities: added NO_2 (▲), NO_2 produced in the $O_3 + NO$ reaction (*), HNO_3 produced in the $OH + NO_2$ reaction (■) and background at *m*/*e* 82 (□).

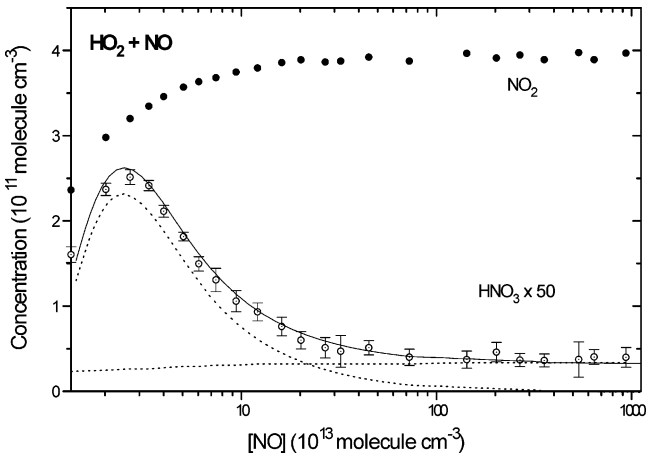

Figure 5. Production of NO_2 and HNO_3 in the $HO_2 + NO$ reaction as a function of NO concentration at 298 K. Dotted curves are separately calculated for HNO_3 from reactions 5 and 1b; solid curve is their sum.

until the complete conversion of HO_2 to NO_2 in reaction 1a, reaching a constant value of $[NO_2]_f = 3.9 \times 10^{11}$ molecule cm^{-3}. The increase of HNO_3 concentration due to reaction 5

$$OH + NO_2 + M \rightarrow HNO_3 + M \qquad (5)$$

is followed by its decrease because of more important consumption of OH in reaction 4 at higher [NO]

$$OH + NO + M \rightarrow HONO + M \qquad (4)$$

down to a constant nonzero level of $[HNO_3]_f = 8 \times 10^8$ molecule cm^{-3}. The branching ratio for the HNO_3-forming channel of the primary $HO_2 + NO$ reaction was determined as a ratio of concentrations of the formed HNO_3 to the formed NO_2, $\beta = [HNO_3]_f/[NO_2]_f = 2.05 \times 10^{-3}$ at high NO concentrations corresponding to the total consumption of OH in the reaction 4. Table 3 summarizes the measurements at 298 K in the absence of water. The experiments which have been performed during a long period are placed in chronological order. A change of the relative sensitivity (I_{82}/I_{46}) is clearly seen after a change of the operating regime of the ion source. The average value obtained from 16 experiments with excess NO is $\beta = (1.66^{+0.40}_{-0.60}) \times 10^{-3}$. The indicated error is a combination of the mean standard deviation ($\sigma = 0.32 \times 10^{-3}$) and the systematic uncertainty of the ratio of HNO_3 to NO_2 sensitivities

TABLE 3: Branching Ratio, β, for the HNO_3-Forming Channel in the $HO_2 + NO$ Reaction at 298 K

I. OH scavenging by NO; $\alpha^a = k_5 \cdot [NO_2]_{tot}/k_4 \cdot [NO]$

[NO] 10^{15}	$[NO_2]_{bgr}$ 10^{11}	$\Delta[NO_2]$ 10^{11}	$[NO_2]_{tot}$ 10^{11}	$\Delta[HNO_3]$ 10^8	β %	I_{82}/I_{46} %	α^a %
3.6	0.94	3.3	4.2	6.9	0.208	1.34	0.025
3.1	2.7	5.0	7.7	10.5	0.213	1.75	0.053
3.9	6.0	4.8	10.8	8.5	0.180	1.07	0.059
9.4	4.9	3.9	8.8	8.0	0.205	1.54	0.020
2.0	6.0	6.0	12.0	11.6	0.194	1.33	0.128
12.3	1.3	2.2	3.5	3.9	0.176	0.59	0.006
9.4	1.1	2.3	3.3	4.9	0.216	0.70	0.008
9.3	1.8	5.2	7.0	5.4	0.104	0.40	0.017
6.2	1.4	5.7	7.1	7.5	0.133	0.50	0.024
6.2	5.0	8.5	13.5	12.2	0.143	0.60	0.046
7.0	3.1	14.4	17.5	16.1	0.112	0.52	0.053
17	5.4	4.9	10.3	8.5	0.171	0.65	0.013
9.3	1.3	3.9	5.2	5.1	0.129	0.57	0.012
9.3	1.2	4.6	5.8	6.9	0.150	0.70	0.013
9.3	3.3	1.5	4.8	2.9	0.197	0.92	0.011
10.8	0.7	1.3	2.0	1.7	0.137	0.60	0.004
			average: 0.166 ± 0.037				

II. OH scavenging by C_6H_{12}; $\alpha^a = k_5 \cdot [NO_2]_{tot}/k_6 \cdot [C_6H_{12}]$

$[C_6H_{12}]$ 10^{15}	$[NO_2]_{bgr}$ 10^{11}	$\Delta[NO_2]$ 10^{11}	$[NO_2]_{tot}$ 10^{11}	$\Delta[HNO_3]$ 10^8	β %	I_{82}/I_{46} %	α^b %
13.2	25	10.4	35	20.0	0.191	1.22	0.056
3.6	1.1	2.2	3.3	3.1	0.162	0.81	0.008
14.2	2.1	1.4	4.8	2.9	0.203	0.95	0.0062
			average: 0.185 ± 0.017				

[a] α is the upper limit of the probability of HNO_3 formation in the side $OH + NO_2$ reaction; concentrations are in units of molecule cm^{-3}.

determined from the yield of HNO_3 in reaction 5, as discussed above. In this way, systematic errors in the determination of NO_2 concentration do not affect the obtained branching ratio.

At [NO] > 5×10^{15} molecule cm^{-3} the relative rate of HNO_3 formation from OH in reaction 5 is less than $\alpha = k_5 \cdot [NO_2]/k_4 \cdot [NO] = 1.6 \times 10^{-4}$, which is less than 10% of the measured HNO_3 yield, and was neglected. The range of the measured HNO_3 concentrations from reaction 1 was $(3-16) \times 10^8$ molecule cm^{-3}, well above the HNO_3 detection limit discussed above.

A strong indication that the observed product is effectively HNO_3 was obtained from comparison of its detection sensitivities using SF_6^- and SiF_5^-, with that for HNO_3. As the detection limit increases strongly with switching from SF_6^- to SiF_5^-, detection of the product from 1b with SiF_5^- was made after a careful optimization of the parameters of the ion source and ion optics. This allowed us to attain the sensitivities of 2.0×10^7 molecule cm^{-3}/cps (NO_2) and 3.9×10^6 molecule cm^{-3}/cps (HNO_3) when they were detected by reaction with SF_6^-. These values were obtained from the calibration using $H + NO_2$ reaction with $[NO_2] = 1.4 \times 10^{13}$ molecule cm^{-3} (see part II in Table 2). When half of SF_6^- ions were converted to SiF_5^-, the signals changed as in the previous experiment (part I). The signal intensities at *m*/*e* 46, 82, and 186 measured in the course of the $HO_2 + NO$ reaction (discharge on−off difference) are presented in parts III and IV of Table 2.

Part III of Table 2 corresponds to [NO] = 9.3×10^{14} molecule cm^{-3} with incomplete scavenging of OH radicals. Here the HNO_3 signal consists of the contributions from both reactions 1b and 5. The sensitivity ratio of this combined signal with respect to detection by SF_6^- to SF_5^- is 20.7 ± 5.0. Part IV of Table 2 corresponds to [NO] = 9.3×10^{15} molecule cm^{-3}, and the sensitivity ratio becomes 18.4 ± 6.1. The latter two

values can be compared with the sensitivity ratio of 22.9 ± 1.0 obtained for HNO_3. Although the error limits of the obtained sensitivity ratios are rather high, it is likely that only one and the same compound is detected in the three cases.

3.2. Detection of HNO_3 Using OH Scavenging by C_6H_{12}. Kinetic behavior of HO_2 radicals and the OH, NO_2, and HNO_3 reaction products in the HO_2 + NO chemical system with [NO] = 2.5×10^{13} and [HO_2] = 2.8×10^{11} molecule cm^{-3} is shown in Figure 6a. The measured concentrations well agree with the results of the numerical integration presented by solid curves. Reactions used in the calculation are listed in Table 1. The changes in the kinetic curves shown in Figure 6b are a result of the addition of about 4×10^{15} molecule cm^{-3} of cyclohexane to the reaction mixture. The most important change is the increase of NO_2 concentration by more than a factor of 3. Formation of extra NO_2 is explained by the subsequent reactions of the cyclohexyl radical, C_6H_{11}, in the presence of NO and large concentrations of O_2 (3.3×10^{15} molecule cm^{-3}):

$$OH + C_6H_{12} \rightarrow C_6H_{11} + H_2O \quad (6)$$

$$C_6H_{11} + O_2 + M \rightarrow C_6H_{11}O_2 + M \quad (8)$$

$$C_6H_{11}O_2 + NO \rightarrow C_6H_{11}O + NO_2 \quad (9)$$

Platz et al.[29] have shown that the cyclic $C_6H_{11}O$ radical under our conditions isomerizes to the linear $HC(O)(CH_2)_4\dot{C}H_2$ radical:

$$C_6H_{11}O \rightarrow HC(O)(CH_2)_4\dot{C}H_2 \quad (10)$$

The further oxidation mechanism of this radical in excess of NO over NO_2 is the following:[30]

$$HC(O)(CH_2)_4\dot{C}H_2 + O_2 \rightarrow HC(O)(CH_2)_4CH_2O_2 \quad (11)$$

$$HC(O)(CH_2)_4CH_2O_2 + NO \rightarrow HC(O)(CH_2)_4CH_2O + NO_2 \quad (12)$$

$$HC(O)(CH_2)_4CH_2O \rightarrow HC(O)CH_2\dot{C}H(CH_2)_2CH_2OH \quad (13)$$

$$HC(O)CH_2\dot{C}H(CH_2)_2CH_2OH + O_2 \rightarrow HC(O)CH_2CH(OO)(CH_2)_2CH_2OH \quad (14)$$

$$HC(O)CH_2CH(OO)(CH_2)_2CH_2OH + NO \rightarrow HC(O)CH_2CH(O)(CH_2)_2CH_2OH + NO_2 \quad (15)$$

$$HC(O)CH_2CH(O)(CH_2)_2CH_2OH \rightarrow HC(O)CH_2CH(OH)(CH_2)_2\dot{C}HOH \quad (16)$$

$$HC(O)CH_2CH(OH)(CH_2)_2\dot{C}HOH + O_2 \rightarrow HC(O)CH_2CH(OH)(CH_2)_2CHO + HO_2 \quad (17)$$

Reactions with O_2 producing HO_2 compete with the isomerization reactions 13 and 16. Termination reactions with NO and NO_2 are not presented for simplicity. HO_2 produced in reaction 17 will regenerate OH through reaction 1 and, thus, creates a chain, in which one HO_2 molecule is produced per four NO_2 molecules (this ratio can somewhat differ due to omitted reactions). The increase of HNO_3 signal with time agrees with its supposed formation in the primary reaction 1. Solid curves in Figure 6b were calculated with the rate constants given in Table 1. As many rate constants in the cyclohexane oxidation are not known, assumptions were made. A value of 7×10^{-12} cm^3 molecule^{-1} s^{-1} was used for the radical + O_2 addition reactions 11 and 14. The rate constants of the isomerization reactions 13 and 16 were assumed to be the same as that of reaction 10. The rate constants taken for reactions 12 and 15

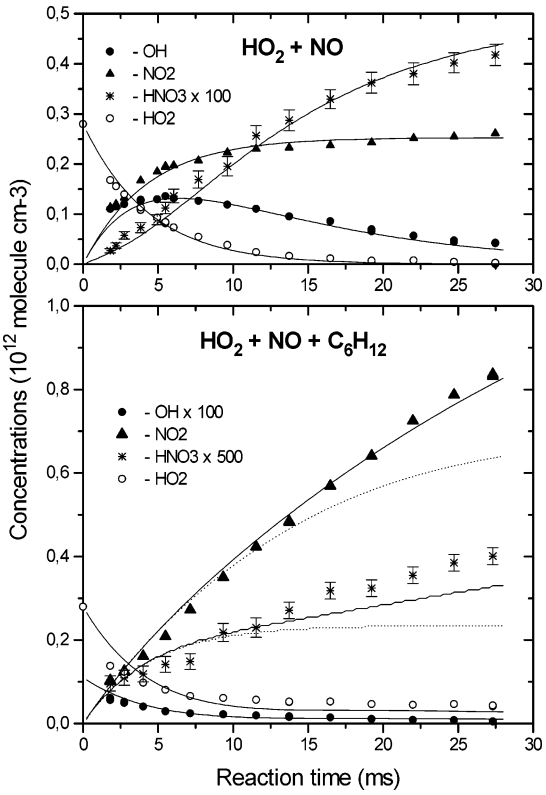

Figure 6. Concentration−time profiles of the species in the HO_2 + NO reaction. (Bottom panel) In the presence of C_6H_{12}. Dotted curves correspond to the absence of the chain (see text).

were that of reaction 9, and a 16% branching ratio for formation of nitrates in reactions 9, 12, and 15 was accounted in the calculation.[29] A value of $k_{17} = 2.6 \times 10^{-11}$ cm^3 molecule^{-1} s^{-1} was taken for reaction 17 by analogy with the reaction C_2H_5-$CHOH + O_2 \rightarrow C_2H_5CHO + HO_2$.[31] Dotted curves in Figure 6 were calculated with $k_{17} = 0$ and show concentrations in the absence of the chain, with HNO_3 only from the primary step.

The branching ratio of reaction 1b can be determined as a ratio of the HNO_3 to NO_2 produced in the initial period of reaction 1 (Figure 6b). The four initial points from this experiment give an average value of $(1.62 \pm 0.22) \times 10^{-3}$. Formation of HNO_3 in OH + NO_2 reaction even for the highest NO_2 concentration formed in this experiment was $\alpha = k_5 \cdot [NO_2]/k_6 \cdot [C_6H_{12}] = 7.8 \times 10^{-5}$, which is less than 5% of the obtained branching ratio. Table 3 presents results of the three experiments with cyclohexane. The average branching ratio is $(1.85 \pm 0.17) \times 10^{-3}$, in good agreement with that obtained from OH scavenging by NO. A mean value of $(0.18^{+0.04}_{-0.06})$% from both methods with error limits including uncertainty in the calibration is recommended.

3.3. Detection of HNO_3 in the Presence of Water Vapor. Water vapor was introduced in the reactor upstream of the injector position fixed at a distance of 50 cm. In one of the experiments, mass spectral response at *m*/*e* 46 and 82 at different water concentrations was measured with OH scavenging by cyclohexane. The initial concentrations in this experiment were [C_6H_{12}] = 3.9×10^{15}, [NO] = 2.5×10^{13}, and [HO_2] = 2.2×10^{11} molecule cm^{-3}. Bohm and Zetzsch[8] determined that the rate constant of reaction 1 does not change in the presence of water which means that the concentration of the formed NO_2 in the predominant channel also does not change in the presence of water. The observed NO_2 signal decreased and background at *m*/*e* 82 increased in agreement with the calibration tests. The dependence of the branching ratio k_{1b}/k_{1a} on [H_2O] was

TABLE 4: Branching Ratio, β, for Formation of HNO_3 in the $HO_2 + NO$ Reaction at 298 K in the Presence of Water[a]

I. $[C_6H_{12}] = 3.9 \times 10^{15}$; $[NO] = 2.5 \times 10^{13}$; $\Delta[NO_2] = 1.3 \times 10^{12}$; $\Delta[HNO_3] = 8.0 \times 10^8$							
$[H_2O]$	0	1.4	2.8	4.3	5.9	8.1	
β (%)	0.162	0.205	0.238	0.247	0.273	0.281	
II. $[NO] = 3.1 \times 10^{15}$; $\Delta[NO_2] = 5.0 \times 10^{11}$							
$[H_2O]$	0	1.09	2.33	4.55	5.95		
β (%)	0.213	0.197	0.207	0.225	0.263		
III. $[NO] = 6.2 \times 10^{15}$; $\Delta[NO_2] = 8.5 \times 10^{11}$							
$[H_2O]$	0	1.07	2.26	3.71	5.39	6.86	7.62
β (%)	0.143	0.147	0.157	0.166	0.176	0.195	0.216
IV. $[NO] = 4.5 \times 10^{15}$; $\Delta[NO_2] = 3.3 \times 10^{11}$							
$[H_2O]$	0	5.96	9.13	9.35	9.77	11.7	
β (%)	0.208	0.295	0.343	0.310	0.328	0.393	
V. $[NO] = 17 \times 10^{15}$; $\Delta[NO_2] = 4.9 \times 10^{11}$							
$[H_2O]$	0	6.0	11.0				
β (%)	0.171	0.215	0.271				
VI. $[NO] = 9.3 \times 10^{15}$; $\Delta[NO_2] = 4.6 \times 10^{11}$							
$[H_2O]$	0	5.07					
β (%)	0.150	0.212					

[a] Concentrations are in units of molecule cm^{-3}; water concentration is in units of 10^{16} molecule cm^{-3}.

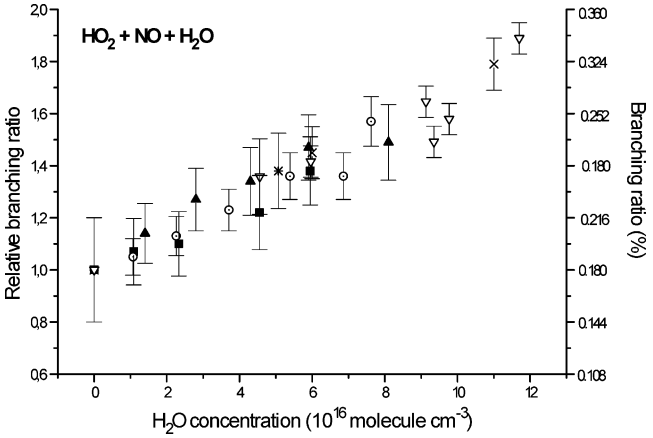

Figure 7. Water effect on the branching ratio of the HNO_3-forming channel of the $HO_2 + NO$ reaction. Different symbols denote separate experiments.

determined from the ratio of the HNO_3 to NO_2 signals assuming independence of the ratio of NO_2 to HNO_3 sensitivities on the concentration of H_2O. The results of this experiment are given in the first entry of Table 4. All other measurements presented in Table 4 were done employing NO as an OH quencher. Figure 7 is a plot of the measured values of β against $[H_2O]$. Each experiment from Table 4 is presented in different symbols. Figure 7 shows that β linearly increases with the increase of water concentration with the maximal increase by 90% at $[H_2O] = 1.17 \times 10^{17}$ molecule cm^{-3}.

3.4. Temperature Dependence of the Branching Ratio. The branching ratio of reaction 1 at temperatures between 298 and 223 K was measured in order to determine the rate constant of the HNO_3-forming channel for conditions relevant to the upper troposphere. Three experiments were performed at a high NO concentration of $[NO] = 9.3 \times 10^{15}$ molecule cm^{-3} and reaction time from 15 to 30 ms. A constant pressure of 200 Torr was kept in the reactor when the main flow was cooled. Figure 8a represents the obtained dependence $\beta(T)$, while Figure 8b shows the data in Arrhenius form. Different symbols denote separate experiments. The cumulative results of these experiments are given in Table 5. Nearly a 5-fold increase of the branching ratio β was found when the temperature was lowered across this range. It was found that the rate constant increases from $k_{1b} = (1.6 \pm 0.5) \times 10^{-14}$ cm^3 $molecule^{-1}$ s^{-1} at 298 K to

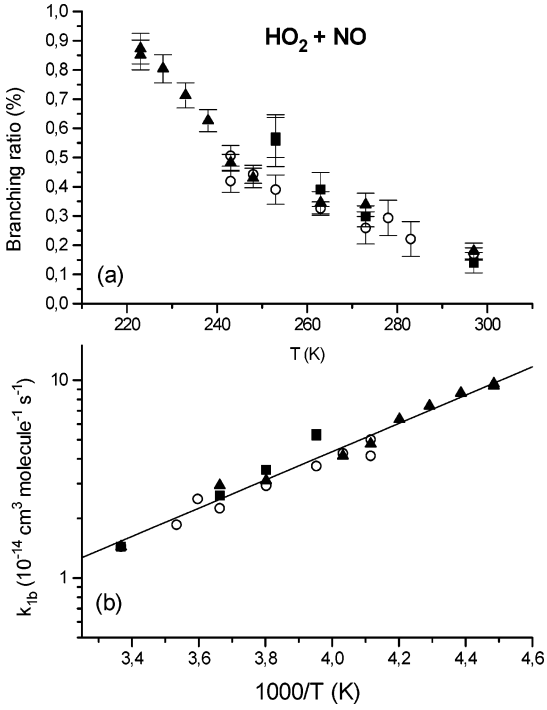

Figure 8. Temperature dependence of the branching ratio of the HNO_3-forming channel of the $HO_2 + NO$ reaction (a) and Arrhenius plot for k_{1b} (b).

TABLE 5: Temperature Dependence of the Branching Ratio, $\beta = k_{1b}/k_{1a}$, and the Rate Constant k_{1b} for $HO_2 + NO$ Reaction[a]

T (K)	β (%)	k_1 $(10^{-12})^b$	k_{1b} (10^{-14})
298	0.18 ± 0.06	8.8 ± 1.2	1.6 ± 0.5
283	0.22 ± 0.06	9.3 ± 1.3	2.0 ± 0.6
273	0.30 ± 0.06	9.6 ± 1.3	2.9 ± 0.7
263	0.35 ± 0.07	9.9 ± 1.4	3.5 ± 0.8
253	0.41 ± 0.07	10.3 ± 1.4	4.2 ± 0.9
243	0.52 ± 0.07	10.8 ± 1.5	5.6 ± 1.0
233	0.71 ± 0.08	11.3 ± 1.6	8.0 ± 1.4
223	0.87 ± 0.08	11.9 ± 1.7	10.4 ± 1.7

[a] Rate constants are in units of cm^3 $molecule^{-1}$ s^{-1}. [b] Reference 10.

$(10.4 \pm 1.7) \times 10^{-14}$ cm^3 $molecule^{-1}$ s^{-1} at 223 K. In the 223−300 K range the rate constant of the HNO_3-forming channel can be expressed as

$$k_{1b} = 6.4 \times 10^{-17} \exp((1644 \pm 76)/T)\ \text{cm}^3\ \text{molecule}^{-1}\ \text{s}^{-1}$$

The mechanism of HNO_3 formation explaining the obtained strong negative temperature dependence of k_{1b} and its atmospheric impact are discussed below.

4. Discussion

4.1. Other Possible Contributions to the Signal at *m/e* 82. To assign the signal observed at *m/e* 82 during reaction 1 entirely to the products of the gas-phase reaction, we had to verify that switching on the discharge did not lead to the appearance of other contributions to this mass peak. The possible causes of such contributions could be unknown processes in the IMR (ion source), formation of nitric acid from the trace NO_2 in the injector, and reactions on the surface of the reactor. Different tests were done which showed that the discharge products do not interfere with signal at *m/e* 82. In particular, this was checked for the discharge in He or H_2/He flow, with or without O_2 in the injector. As well, no change of signal at *m/e* 82 was observed in the absence of O_2 flow through the injector with turning on the discharge in He or the H_2/He mixture when NO was flowing through the reactor. Although formation of small amounts of O-atoms and/or OH radicals was sometimes registered in the discharge of He flow, it means that possible oxygen and water impurities in He did not lead to formation of HNO_3. It also means that possible formation of HNO_3 from the trace background NO_2 (e.g., degassing of viton inlet tubings) was below the detection limit.

Two mechanisms can be considered for the possible formation of HNO_3 on the reactor wall: (i) the diffusion of the radicals (OH or HO_2) to the wall and their conversion to HNO_3 on the surface and (ii) the transport of the radicals to the surface during the initial mixing process.

The former mechanism (i) can be excluded on the following basis: the NO concentration in our experiments was higher than 10^{16} molecule cm^{-3} corresponding to first-order reaction rates higher than 10^5 s^{-1} for both OH and HO_2 radicals. The maximum wall loss rates observed in our experiments for these radicals were less than 15 s^{-1}. Comparing these rates, the maximum yield of any product of radicals conversion on the wall of the reactor cannot be higher than 2×10^{-4}, and hence, this mechanism cannot be responsible for the observed 2×10^{-3} yield of HNO_3 at 298 K. Another argument supporting the unimportance of this mechanism is the pressure dependence of the HNO_3 yield. Figure 9 presents the branching ratio measured in excess of NO at pressures of 100, 200, 300, and 400 Torr. The measurements were done at room temperature with [NO] = $(0.9-1.2) \times 10^{16}$ and $[HO_2]_0 = 5 \times 10^{11}$ molecule cm^{-3}. The results show positive linear pressure dependence incompatible with the heterogeneous formation of HNO_3. Under the conditions of our turbulent reactor, the limiting process determining the rate of wall loss of the radicals is the diffusion of the radicals through the laminar layer near the reactor wall. As the turbulent conditions in the reaction region are not stationary (that is the turbulence parameters are not constant along the reactor), the thickness of this layer cannot be easily estimated theoretically. However, assuming that the thickness is independent of pressure, the wall loss should be slower at higher pressures, and consequently, the yield of HNO_3, in case of its formation from radical conversion on the surface, would be lower.

The latter mechanism (ii) can be ruled out taking into account that in the HO_2 + NO + C_6H_{12} system the radicals are regenerated along the length of the entire reaction zone, and hence, the HNO_3 formation cannot be explained by the possibility for radicals to reach the surface during the initial mixing process. We have performed a large number of experiments in which the influence of the injector flow rate on the mixing of injector and main reactor components has been investigated. As a result of these experiments, we use the flow rate which corresponds to the most homogeneous distribution at shortest reaction times. The experiments were performed with stable species (NO, NO_2, O_3) as well as with radicals (OH, F, O) being flowed through the injector. Accounting for the homogeneous losses in the case of the radicals, the observed concentration profiles allow us to exclude the possibility of radical losses during the initial mixing process at the used injector flow rates.

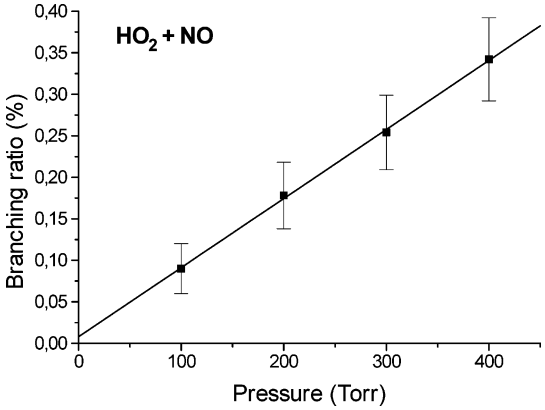

Figure 9. Pressure dependence of the branching ratio of the HNO_3-forming channel of the HO_2 + NO reaction at 298 K with $[HO_2]_0 = 5 \times 10^{11}$ molecule cm^{-3}. The error limits correspond to systematic errors in the measurement of the signals and uncertainties in the calibration of the HNO_3 to NO_2 signal ratio.

Another question is a possible contribution to the signal at *m/e* 82 from NO_2 produced in reaction 1. This was tested using the reaction of ozone with NO yielding NO_2 in situ under conditions similar to that used during the study of reaction 1 including maintenance of the same O_2 and H_2 flow rates:

$$O_3 + NO \rightarrow NO_2 + O_2 \qquad (18)$$

Reaction 18 was held in a large excess of NO, and different concentrations of NO_2 were obtained by varying the ozone concentration. No change of the background level at *m/e* 82 was observed in the range of $[O_3] = 3 \times 10^{11}-5 \times 10^{12}$ molecule cm^{-3}. These experiments proved that formation of NO_2 in the reactor does not yield an increase of the signal at *m/e* 82.

4.2. Mechanism of the HNO_3 Formation and Theoretical Models. The HO_2 + NO reaction is the first member of the RO_2 + NO reaction family, proceeding via the ROONO intermediate with subsequent branching to RO + NO_2 or to $RONO_2$ products. It is interesting to discuss the obtained branching ratio for HNO_3 formation in reaction 1, $k_{1b}/k_{1a} = 0.18\%$ at 298 K, in view of the existing experimental[33-37] and theoretical[38-43] studies of the $RONO_2$ yields from alkyl peroxy radical reactions with NO. Table 6 shows experimental results of the $RONO_2$ formation for small *n*-alkyl peroxy radicals. Very small yields were observed for C_2 and C_3 nitrates. Starting from C_5, the yield increases monotonically approaching a limit of ~35% at 298 K for large *n*-alkyl peroxy radicals.[37] As has been already mentioned, formation of HNO_3 in the HO_2 + NO reaction has never been observed previously, and early ab initio calculations explained this by a high barrier for isomerization of HOONO to HNO_3.

TABLE 6: Literature Data on RO_2 + NO Branching Ratios for $RONO_2$ Formation, β, from the Product Studies at 100 < *P* < 200 Torr

RO_2 reactant	$\beta(T)$	*T*, K	$\beta(T)$	*T*, K	*P*, Torr	detected products	method	ref
HO_2	0.0018	298	0.0087	223	200	HNO_3	HPTFR/CIMS	this work
CH_3O_2	<0.03	295			100	CH_3ONO_2	HPTFR/CIMS	32
	<0.1	300	<0.1	193	100−200	CH_3O_2, NO_2	HPTFR/CIMS	33
$C_2H_5O_2$	0.006	298	0.02	213	100	$C_2H_5ONO_2$	HPTFR/CIMS	34
$C_3H_7O_2$	0.006	298	0.02	213	100	$C_3H_7ONO_2$	HPTFR/CIMS	35
$C_5H_{11}O_2$	0.038	327	0.068	284	155	$C_5H_{11}ONO_2$	PR/GC FID[a]	36

[a] Photoreactor and gas chromatography with flame ionization detection.

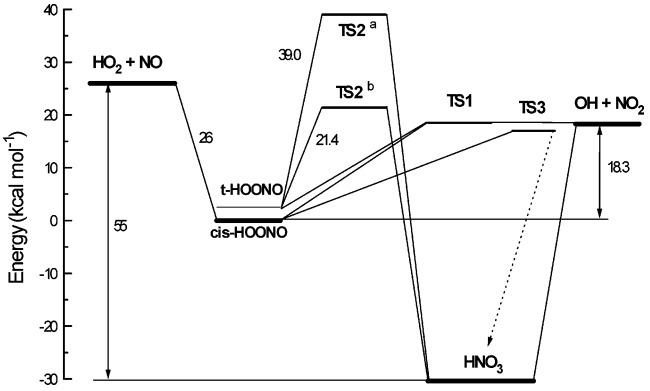

Figure 10. Energy diagram for HO_2 + NO system. TS2, transition state for isomerization as calculated in refs 38 (a) and 39 (b); TS3, transition state for isomerization.[22,42] Other indicated energies are from ref 44.

Figure 10 presents the energy diagram for the HO_2 + NO system. Reaction starts with formation of the HOONO complex bound by 26 kcal mol^{-1} as calculated by Li and Francisco at the QCISD(T)cc-pVQZ level of theory.[44] It is important that the complex has two major conformations: cyclic *cis*-structure and nearly linear *trans*-structure separated by a 16 kcal mol^{-1} barrier (not shown), *trans*-conformer lying ~3 kcal mol^{-1} higher.[21,22] The dissociation energy is 18 ± 1 kcal mol^{-1}.[21,44] This energy diagram is generic for the RO_2 + NO family, the dissociation energy varying systematically, with H highest, CH_3 lowest, and C_2 and heavier R between.[43] Activated HOONO** complex can unimolecularly decompose to OH + NO_2 (TS1) or isomerize to HNO_3 (TS2). A key parameter for the isomerization/dissociation branching ratio is a barrier of the transition state for isomerization (TS2). In the early study employing the MP4SDQ/6-31G* method, the TS2 was found to lie 60 kcal mol^{-1} higher than HOONO.[45] The calculation by Sumathi and Peyerimhoff[38] and more recently by Lohr et al.,[40] both using the DFT B3LYP/6-31G++** method, gave 39.0 kcal mol^{-1}. Calculation of Dixon et al. at the CCSD(T) level of theory gave a substantially lower barrier height of 21.4 kcal mol^{-1}.[39] In all these calculations the reaction path was a direct migration of the OH group from oxygen to nitrogen in *trans*-conformer via a three-centered transition state. Although according to the latter calculation this transition state is energetically accessible, it cannot explain a negative temperature dependence of k_{1b} as observed in the present work. A possible explanation of this dependence can be found in the study of Dransfield et al.[22] where the isomerization to HNO_3 via an OH + NO_2 productlike transition state (TS3) has been suggested. They propose that at TS3 the barrier to internal rotation lies below that of dissociation, and the species may rotate from an HOONO conformation to an $HONO_2$ conformation and relax (dotted arrow in Figure 9). Quite recently, Zhao et al.[42] optimized the minima and transition states (stationary points) on such reaction path using UCCSD(T)/6-31+G* and CBS-QB3 methods. In their study the TS3 arises from the *cis*-HOONO by O−O cleavage and involves the hydrogen bonded OH−ONO intermediate which recombines to nitric acid without a significant barrier. The obtained CBS-QB3 barrier height is 18−19 kcal mol^{-1}.

Even lower barriers were postulated for isomerization transition states in master equation studies of alkyl nitrate formation in RO_2 + NO reaction.[41,43] To simulate experimental results acquired at different temperatures and pressures, the barrier height had to be at least 1 kcal mol^{-1} below the RO + NO_2 asymptotic energy. Then, correct pressure and temperature dependences could be obtained. Specifically, it was obtained that $RONO_2$ yields increase drastically with decreasing temperature. Though in these works the yields were calculated for R=CH_3 and heavier reactants, the general consideration included R=H. The important conclusion from both studies[41,43] is that the temperature effect is determined by the energy difference between TS1 and TS3. Calculations of Zhao et al.[42] support a possibility that the isomerization barrier lies below the dissociation limit, which can explain the negative temperature dependence for the HNO_3 yield observed in the present study.

4.3. Mechanism of HNO_3 Formation in the Presence of H_2O and Chemical Amplifiers. To analyze the role of water in the HO_2 + NO reaction, formation of HO_2·H_2O complex is assumed:

$$HO_2 + H_2O \leftrightarrow HO_2{\cdot}H_2O \qquad (19)$$

The geometry of HO_2·H_2O complex was determined at a high level of ab initio calculations[46] and presents a ring structure with two hydrogen bonds of 6.9 kcal mol^{-1}. The equilibrium constant for reaction 19 is $K_{19} = 3 \times 10^{-19}$ cm^3 $molecule^{-1}$ at 298 K.[47] At water partial pressure of 3 Torr, $[HO_2{\cdot}H_2O]/[HO_2] = K_{19}[H_2O] = 0.036$; i.e., about 4% of HO_2 in the reactor are in the form of the complex. It can be calculated that the observed effect of approximate doubling the HNO_3 yield in reaction 1 with 3 Torr of H_2O can be achieved if the yield of HNO_3 in the HO_2·H_2O + NO reaction is as high as ~5%. Let us consider possible mechanisms.

The NO approach from the side of any oxygen atom belonging to HO_2 will most probably lead to elimination of water and formation of HOONO complex bound by ~26 kcal mol^{-1} [44] and probably a less energized HOONO complex than that formed in reaction 1 because H_2O molecule can carry away a part of the released energy:

$$HO_2{\cdot}H_2O + NO \rightarrow [HO_2NO{\cdot}H_2O]^* \rightarrow HOONO^* + H_2O \qquad (20)$$

This case is similar to the catalytic role of water in the HO_2 self-reaction, where an H_2O molecule helps to produce a less excited $(HO_2)_2$ dimer, increasing the rate of formation of H_2O_2 + O_2 products.[48] Like in reaction 1, low-energized HOONO* complex in reaction 20 can decompose to OH + NO_2 or isomerize to HNO_3. Then, the question is how the isomerization

to decomposition branching ratio depends on the activation energy of HOONO complex. Recent theoretical studies of the RO_2 + NO reactions[41,43] suggest that decomposition dominates at initial activation energy (HOONO**), but with a decrease of the excitation, dissociation rate constant will decrease more rapidly than the isomerization rate constant, so that at low energies (below the dissociation limit) isomerization dominates. Evidently, HOONO* activation is somewhere between the reactant (HO_2 + NO) and radical product (OH + NO_2) energy limits, and we observe a change of the branching ratio from 0.18% (dry case) to ~5% (participation of H_2O). Explicit calculations of the microcanonical rate constants for decomposition and isomerization as a function of energy for R = C_5H_{11}[41,43] indicate that this change is realistic for R=H.

As an alternative mechanism, it was suggested that H_2O promotes production of HNO_3 in a peroxy radical amplifier by lowering the rearrangement barrier:[4]

$$HO_2{\cdot}nH_2O + NO \rightarrow HONO_2 + nH_2O \qquad (21)$$

The mechanism with $n = 2$ was developed to explain a quadratic decrease of chain length with the increase of relative humidity found in that study. However, this disagrees with our results giving linear dependence of the HNO_3 yield on water concentration. Generally, mechanism of such concerted isomerization with $n = 1$ can be imagined assuming a seven-membered transition state, and additional ab initio calculations are needed to test this possibility. Michele et al. also reported a linear decrease of the chain length in the radical amplifier in the presence of wet air.[2] They calculated that a rate coefficient of about 7×10^{-13} cm^3 $molecule^{-1}$ s^{-1} for the second-order reaction of the $HO_2{\cdot}H_2O$ adduct with NO giving a nonradical product would explain their observations. Since the HO_2 + NO reaction rate does not change in the presence of water, it means that the required branching ratio k_{20}/k_{1a} should be about $7 \times 10^{-13}/8.8 \times 10^{-12}$ = 8% which is consistent with our value of ~5%.

4.4. Atmospheric Implication. Channel 1b forming HNO_3 in the HO_2 + NO reaction becomes a new potentially significant loss process for the HO_x (OH, HO_2) radicals in the atmosphere. In the troposphere the OH and HO_2 radicals are recycled through the reactions

$$OH + CO, CH_4, NMHC + O_2 \rightarrow HO_2$$

$$HO_2 + NO \rightarrow OH + NO_2 \qquad (1a)$$

and reaction 1a leads to ozone formation through photolysis of NO_2 and further reaction of the formed O-atoms with O_2. Hence, the HO_x loss processes reduce ozone formation [e.g., 49].

In the lower troposphere the major HO_x loss under NO_x "rich" conditions is reaction

$$OH + NO_2 + M \rightarrow HNO_3 + M \qquad (5)$$

nitric acid being taken up by water aerosols and mostly washed out by precipitations. The significance of reaction 1b as the HO_x loss process can be assessed by calculating the relative rate ratio of reactions 1b and 5: $r = k_{1b}[HO_2][NO]/k_5[OH][NO_2]$. Such expression is valid considering the OH/HO_2 conversion being fast compared to HO_x loss. Using $k_{1b} = 1.6 \times 10^{-14}$ cm^3 $molecule^{-1}$ s^{-1} at 298 K from this work, $k_5 = 1.1 \times 10^{-11}$ cm^3 $molecule^{-1}$ s^{-1} at 298 K, 1 atm,[17] and typical values for the lower troposphere [NO]/[NO_2] ≈ 0.5 and [HO_2]/[OH] ≈ 50, we obtain $r \approx 2\%$. Even considering the rather large variability of [NO]/[NO_2] and [HO_2]/[OH] ratios, reaction 1b should not contribute significantly to the HO_x loss in the lower troposphere.

TABLE 7: Measured Concentrations of Species[a] and Main HO_x Loss Rates in the Upper Troposphere

	concentration (pptv)	
species	marine air	continental air
OH	0.1	0.1
HO_2	4.7	1.1
NO	49	443
NO_2	11	163
HNO_3	44	130
HO_2NO_2	40	63

HO_x loss	rate constant[b] cm^3 $molecule^{-1}$ s^{-1}	loss rate molecule cm^{-3}/s	
OH+HO_2 → H_2O+O_2	1.5×10^{-10}	1.2×10^4	2.8×10^3
HO_2+HO_2 → H_2O_2	4.2×10^{-12}	1.6×10^4	8.9×10^2
OH + HO_2NO_2 → H_2O+NO_2+O_2	6.4×10^{-12}	2.2×10^3	3.5×10^3
OH+NO_2 → HNO_3	7.4×10^{-12}	7.1×10^2	1.0×10^4
OH + HNO_3 → H_2O + NO_3	5.8×10^{-13}	2.2×10^2	6.6×10^2
Total:	3.1×10^4	1.8×10^4	
HO_2 + NO → HNO_3	1.0×10^{-13}[c]	2.0×10^3	4.3×10^3
HO_2 + NO → HNO_3 (% of total loss)		**6.4**	**23**

[a] From the SONEX aircraft campaign (T = 223 K and P = 260 Torr).[50] [b] Rate constants are from ref 10. [c] This work.

The situation can be different in the upper troposphere, due to the much higher values of the [NO]/[NO_2] ratios and of the rate constant of reaction 1b at low temperature. Considering the UT at an ~10 km altitude with typical conditions T = 223 K and P = 260 Torr, we have used concentrations data of the SONEX campaign[50] to compare reaction 1b with the known HO_x loss processes. Table 7 contains the results of the aircraft measurements for low-NO_x (marine) and high-NO_x (continental) atmospheric regimes as well as calculated rates for the most important reactions leading to the loss of HO_x. We see that reaction 1b contributes 23% of the total HO_x loss for high-NO_x conditions. Even in the low-NO_x regime with predominant loss via the OH + HO_2 and HO_2 + HO_2 reactions, the HO_2 + NO loss pathway is not negligible and amounts to about 6% of the total loss.

In conclusion, the HNO_3-forming channel of the HO_2 + NO reaction observed for the first time in this work could be a significant HO_x loss process in the UT with a potential impact on ozone production. The impact of this reaction will be less in the lower troposphere.

Acknowledgment. The study was performed partly in the frame of the SCOUT-O3 integrated EU project. The authors are grateful to Dr. Gerard Laverdet for discussions on chemical amplifier measurements and technical help in experiments.

References and Notes

(1) Hastie, D. R.; Weissenmayer, M.; Burrows, J. P.; Harris, G. W. *Anal. Chem.* **1991**, *63*, 2048.
(2) Mihele, C. M.; Mozurkewich, M.; Hastie, D. R. *Int. J. Chem. Kinet.* **1999**, *31*, 145.
(3) Coll, I.; Pinceloup, S.; Perros, E. P.; Laverdet, G.; Le Bras, G. *J. Atmos. Res.* **2005**, *74*, 477.
(4) Reichert, L.; Hernandez, M. D. A.; Stöbener, D.; Burkert, J.; Burrows, J. P. *J. Geophys. Res.* **2003**, *108*, 4017.
(5) Howard, C. J.; Evenson, K. M. *Geophys. Res. Lett.* **1977**, *4*, 437.
(6) Howard, C. J. *J. Chem. Phys.* **1979**, *71*, 2352.
(7) Seely, J. V.; Meads, R. F.; Elrod, M. J.; Molina, M. J. *J. Phys. Chem.* **1996**, *100*, 4026.
(8) Bohn, B.; Zetzsch, C. *J. Phys. Chem. A* **1997**, *101*, 1488.
(9) Bardwell, M. V.; Bacak, A.; Raventos, M. T.; Percival, C. J.; Sanchez-Reyna, G.; Shallcross, D. E. *Phys. Chem. Chem. Phys.* **2003**, *5*, 2381.

(10) Atkinson, R.; Baulch, D. L.; Cox, R. A.; Crowley, J. N.; Hampson, R. F.; Hynes, R. G.; Jenkin, M. E.; Rossi, M. J.; Troe, J. *Atmos. Chem. Phys*. **2004**, *4*, 1461.
(11) Kukui, A.; Borissenko, D.; Laverdet, G.; LeBras, G. *J. Phys. Chem. A* **2003**, *107*, 5732.
(12) Huey, L. G.; Hanson, D. R.; Howard, C. J. *J. Phys. Chem*. **1995**, *99*, 5001.
(13) (a) Huey, L. G.; Lovejoy, E. R. *Int. J. Mass Spectrom. Ion Processes* **1996**, *155*, 133. (b) Huey, L. G.; Dunlea, E. J.; Lovejoy, E. R.; Hanson, D. R.; Norton, R. B.; Fehsenfeld, F. C.; Howard, C. J. *J. Geophys. Res*. **1998**, *103*, D3, 3355.
(14) Ikezoe, Y.; Matsuoka, S.; Takebe, M.; Viggiano, A. *Gas-Phase Ion*−*Molecule Reaction Rate Constants Through 1986*; Ion Reaction Research Group of the Mass Spectroscopy Society of Japan, Maruzen Company: Tokyo.
(15) Elrod, M. J.; Ranschaert, D. L.; Schneider, N. J. *Int. J. Chem. Kinet.* **2001**, *33*, 363.
(16) Sander, S. P.; Friedl, R. R.; Golden, D. M.; Hampson, R. F.; Kurylo, M. J.; Huie, R. E.; Orkin, V. L.; Moortgat, G. K.; Ravishankara, A. R.; Kolb, C. E.; Molina, M. J.; Finlayson-Pitts, B. J. *Evaluation Number 14*, JPL Publication 02-25; Jet Propulsion Laboratory: Pasadena, CA, 2003.
(17) D'Ottone, L.; Campuzano-Jost, P.; Bauer, D.; Hynes, A. J. *J. Phys. Chem. A* **2001**, *105*, 10538.
(18) Neuman, J. A.; Huey, L. J.; Ryerson, T. B.; Fahey, D. W. *Environ. Sci. Technol*. **1999**, *33*, 1133.
(19) Donahue, N. M.; Mohrschladt, R.; Dransfield, T. J.; Anderson, J. G.; Dubey, M. K. *J. Phys. Chem. A* **2001**, *105*, 1515.
(20) Golden, D. M.; Smith, G. P. *J. Phys. Chem. A* **2000**, *104*, 3991.
(21) Bean, B. D.; Mollner, A. K.; Nizkorodov, S. A.; Nair, G.; Okumura, M.; Sander, S. P.; Peterson, K. A.; Francisco, J. S. *J. Phys. Chem. A* **2003**, *107*, 6974.
(22) Dransfield, T. J.; Donahue, N. M.; Anderson, J. G. *J. Phys. Chem. A* **2001**, *105*, 1507.
(23) Burkholder, J. D.; Hammer, P. D.; Howard, C. J. *J. Phys. Chem*. **1987**, *91*, 2136.
(24) Hippler, H.; Nasterlack, S.; Striebel, F. *Phys. Chem. Chem. Phys.* **2002**, *4*, 2959.
(25) Matheu, D. M.; Green, W. H., Jr., *Int. J. Chem. Kinet.* **2000**, *32*, 245.
(26) Nizkorodov, S. A.; Wennberg, P. O. *J. Phys. Chem. A* **2002**, *106*, 855.
(27) Arnold, S. T.; Viggiano, A. A. *J. Phys. Chem. A.* **2001**, *105*, 3527.
(28) Finlayson-Pitts, B. J.; Wingen, L. M.; Summer, A. L.; Syomin, D.; Ramazan, K. A. *Phys. Chem. Chem. Phys.* **2003**, *5*, 223.
(29) Platz, J.; Sehested, J.; Nielsen, O. J.; Wallington, T. J. *J. Phys. Chem. A* **1999**, *103*, 2688.
(30) Aschmann, S. M.; Chew, A. A.; Arey, J.; Atkinson, R. *J. Phys. Chem. A* **1997**, *101*, 8042.
(31) Miyoshi, A.; Matsui, H.; Washida, N. *J. Phys. Chem*. **1990**, *94*, 3016.
(32) Scholtens, K. W.; Messner, B. M.; Cappa, C. D.; Elrod, M. J. *J. Phys. Chem. A* 1999, *103*, 4378.
(33) Bacak, A.; Bardwell, M. W.; Raventos, M. T.; Percival, C. J.; Sanchez-Reyna, G.; Schallcross, D. E. *J. Phys. Chem. A* **2004**, *108*, 10681.
(34) Ranschaert, D. L.; Schneider, N. J.; Elrod, M. J. *J. Phys. Chem. A* **2000**, *104*, 5758.
(35) Chow, J. M.; Miller, A. M.; Elrod, M. J. *J. Phys. Chem. A* **2003**, *107*, 3040.
(36) Atkinson, R.; Carter, W. P. L.; Winer, A. M. *J. Phys. Chem*. **1983**, *87*, 2012.
(37) Atkinson, R.; Aschmann, S. M.; Carter, W. P. L.; Winer, A. M.; Pitts, J. N., Jr. *J. Phys. Chem*. **1982**, *86*, 4563.
(38) Sumathi, R.; Peyerimhoff, S. D. *J. Chem. Phys*. **1997**, *107*, 1872.
(39) Dixon, D. A.; Feller, D.; Zhan, C.-G.; Francisco, J. S. J. *Phys. Chem. A* **2002**, *106*, 3191.
(40) Lohr, L. L.; Barker, J. R.; Shroll, R. M. *J. Phys. Chem. A* **2003**, *107*, 7429.
(41) Barker, J. R.; Lohr, L. L.; Shroll, R. M.; Reading, S. *J. Phys. Chem. A* **2003**, *107*, 7434.
(42) Zhao, Y.; Houk, K. N.; Olson, L. P. *J. Phys. Chem. A* **2004**, *108*, 5864.
(43) Zhang, J.; Dransfield, T.; Donahue, N. M. *J. Phys. Chem. A* **2004**, *108*, 9082.
(44) Li, Y.; Francisco, J. *J. Chem. Phys*. **2000**, *113*, 7976.
(45) Cameron, D. R.; Borrajo, A. M. P.; Bennett, B. M.; Thatcher, G. R. J. *Can. J. Chem*. **1995**, *73*, 1627.
(46) Aloisio, S.; Francisco, J. S. *J. Phys. Chem. A* **1998**, *102*, 1899.
(47) Sander, S. P.; Peterson, M. E. *J. Phys. Chem*. **1984**, *88*, 1571.
(48) (a) Mozurkewich, M.; Benson, S. *Int. J. Chem. Kinet*. **1985**, *17*, 787. (b) Zhu, R.; Lin, M. C. *Chem. Phys. Lett*. **2002**, *354*, 217.
(49) Ehhalt, D. H. *Gas-Phase Chemistry of the Troposphere*, in: *Global Aspects of Atmospheric Chemistry*; Zellner, R., Ed.; Springer-Verlag: Berlin, 1999.
(50) Jaeglé, L.; Jacob, D. J.; Brune, W. H.; Faloona, I.; Tan, D.; Heikes, B. G.; Kondo, Y.; Sachse G. W.; Anderson, B.; Gregory, G. L.; Singh, H. B.; Pueschel, R.; Ferry, G.; Blake, D. R.; Shetter, R. E. *J. Geophys. Res.* **2000**, *105*, D3, 3877.
(51) Atkinson, R. *Atmos. Chem. Phys.* **2003**, *3*, 2233.